MASSACHUSETTS INSTITUTE OF TECHNOLOGY

APOLLO

GUIDANCE AND NAVIGATION

MIT INSTRUMENTATION LABORATORY

CAMBRIDGE 39, MASSACHUSETTS

MASSACHUSETTS INSTITUTE OF TECHNOLOGY

APOLLO

GUIDANCE AND NAVIGATION

Approved: Milton B. Trageser Date: 3/18/65
MILTON B. TRAGESER, DIRECTOR
APOLLO GUIDANCE AND NAVIGATION PROGRAM

Approved: Roger B. Woodbury Date: 3/19/65
ROGER B. WOODBURY, DEPUTY DIRECTOR
INSTRUMENTATION LABORATORY

E-1687

AN OPTICAL EARTH HORIZON PROFILE BASED UPON TABULATED SOLUTIONS OF CHANDRASEKHAR'S EQUATIONS

by

Dr. Milo Wolff

October 1964

MIT INSTRUMENTATION LABORATORY
CAMBRIDGE 39, MASSACHUSETTS

COPY # 85

ACKNOWLEDGMENT

This report was prepared under DSR Project 55-191, sponsored by the Manned Spacecraft Center of the National Aeronautics and Space Administration through Contract NAS 9-153.

E-1687

AN OPTICAL EARTH HORIZON PROFILE BASED UPON TABULATED SOLUTIONS OF CHANDRASEKHAR'S EQUATIONS

ABSTRACT

Calculations are made of the luminance of the Earth's atmosphere as a function of the altitude of a line of sight from outer space. Results are obtained as a function of ground albedo, sun angle, and wavelength. Application to space navigation is discussed. Graphical solutions are given for many varied parameters. MIT/IL Report E-1634 is preliminary to this report.

by Dr. Milo Wolff

October 1964

Page intentionally left blank

Page intentionally left blank

TABLE OF CONTENTS

Page intentionally left blank

Page intentionally left blank

LIST OF FIGURES*

*All wavelengths should read 4250 Å, not 4000 Å.

INTRODUCTION

When viewed from outer space the edge of the earth is obscured not only by clouds but also by the atmosphere itself which is sufficiently dense as to hide the edge and sometimes the clouds. If the atmosphere is illuminated by the sun, scattering of the sunlight produces the appearance of a blue haze at the edge. The Luminance of the atmosphere as a function of the altitude of a grazing line of sight is termed a horizon profile. For the purposes of space navigation, an accurate profile is needed to establish a reference horizon.

This report describes a calculation of the horizon profile that makes use of pre-computed solutions[(1)*] to the Rayleigh problem of sunlight scattered by a plane-parallel atmosphere. The calculation uses a model of a real mid-latitude atmosphere containing aerosols.

THE PROBLEM

One of the principal optical difficulties in working with the real atmosphere is the large amount of clouds, smoke, and haze at lower altitudes. Optically speaking, the earth is surrounded by a dirty window pane with most of the dirt at the bottom. Luckily for the outside observer, the low altitude dirt is sometimes concealed by the outer atmosphere and the small high altitude contamination is fairly constant so that it can be taken into account.

In postulating mathematical models , a favorite is the exponential because calculations are simplifed by using a scale

---

(1)*Numeral superscripts refer to similarly numbered references in the Bibliography.

height, k, in the equation

$$\beta = \beta_o \, e^{-h/k}$$

Unfortunately, a plot of extinction coefficients versus altitude in Fig. 1 shows that this is not even approximately true except at higher altitudes.

THE MODEL

Figure 1 is the "standard clear atmosphere" calculated by Elterman[2] for a light wavelength of 0.40 micron. He obtained this by adding an aerosol component to the 1962 standard atmosphere and calculating the extinction coefficients for the mixture. A dotted line has been added to his graph to show the correction required for a tropical atmosphere. This correction is associated with the increased atmospheric density which occurs in the region of temperature inversion just below the tropopause. The model of this paper is a modification of Fig. 1. The upper straight line portion is represented by an exponential function with scale height of 6.43 km and extinction, β_o, of 0.456 per scale height. The lower atmosphere portion is considered as a single slab of optical thickness 0.50, that is, it is treated as an integrated whole according to

$$\text{optical thickness} \equiv \int_{\text{ground}}^{\text{high altitude}} \beta \, dh \cong 0.50$$

Luckily, this is one of the tabulated thicknesses of reference 1, thus avoiding a difficult interpolation problem.

METHOD OF CALCULATION

The slab and exponential top layer described above are used to calculate a horizon profile in two parts. In the first part, the slab receives radiation from the sun which is internally

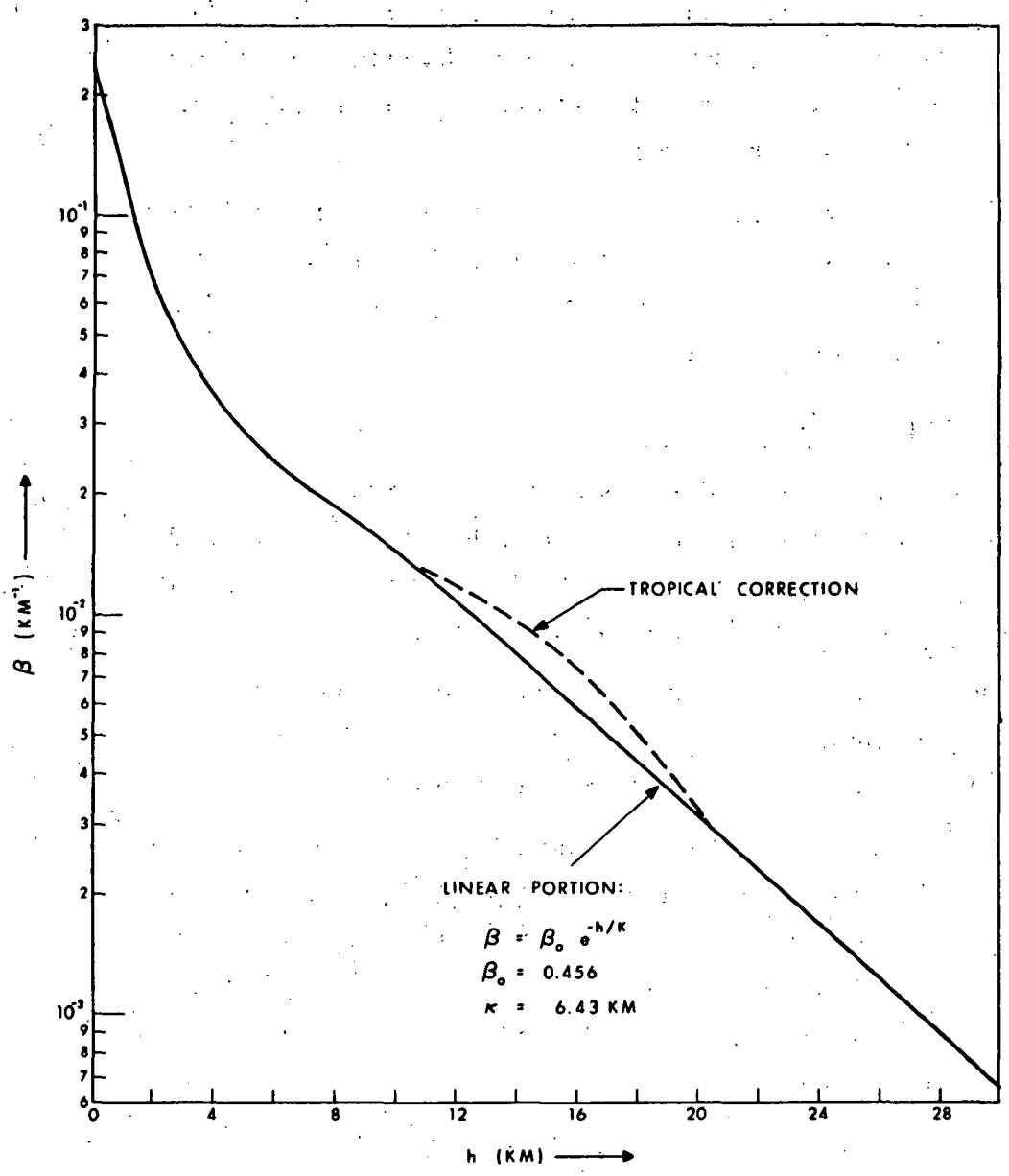

Fig. 1 Extinction coefficient as a function of altitude, for mid-altitudes including typical aerosol content.
From L. Elterman-reference 2..

scattered and reradiated upward into the exponential top layer, where it is again scattered into the line of sight of an outer-space observer. Upward radiation is obtained from the Tables of Coulson, Dave, and Sekera[1] and the top layer scattering is computed here. The second part is the calculation of direct sunlight scattered by the top layer into the line of sight.

In summary, there are two sources of light: the lower slab which radiates upward, and the sun which radiates downward. The light from both sources are scattered by the exponential layer toward the outer-space observer.

COMMENTS ON THE METHOD

It should be recognized that a profile is desired only for line-of-sight altitudes higher than, say, ten kilometers. Indeed, due to the indeterminant nature of the low altitude "dirt", a very accurate profile at low altitude loses meaning.

Because the calculated scattering occurs only in the rarified high atmosphere, multiple scattering is negligible. Thus the single scattering calculation yields good results.

The tabulated solutions of radiation emerging from the lower slab[1] are exact solutions to the Rayleigh problem. Thus they include the effects of multiple scattering in the lower atmosphere. Since solutions are given for various values of ground albedo, sun angle, and optical thickness, these variables may also be treated in this work.

It may be noted that the tabulated solutions apply to a plane-parallel atmosphere, not to a spherical one. However, in this work, they are used as a "local" source and the conversion to the spherical geometry is part of this computation.

MATHEMATICAL DETAILS

The reader may note that a fuller discussion of the horizon profile problem was treated in an earlier report[4] wherein certain

related integrals were derived in detail. These will not be duplicated here.

1. Scattering of the Direct Sunlight

The intensity of the sun's radiation is assumed to be π watts/unit area. In passing through the atmosphere, the intensity is reduced at an altitude z, to

$$I = \pi e^{-Ae^{-z}}$$

where

$$A = \frac{\beta_o}{\mu\left(1 - \frac{2}{\sqrt{2\pi R}}\right) + \frac{2}{\sqrt{2\pi R}}}$$

The amount of light which is rayleigh scattered at an angle of ψ from the incoming sunlight is

$$I_{obs}^{sun} = \frac{1}{4} e^{-Ae^{-z}} \beta_o e^{-z} \left(\frac{3}{4}\right)(1 + \cos^2\psi)\, dx \qquad (1)$$

where dx is an element of length along the line of sight, and the rayleigh scattering angle ψ, is given by

$$\cos\psi = \cos\phi \sin\theta_o$$

Refer to Fig. 2 where the geometry is illustrated.

In order to find the total sunlight which is directly scattered to the outer-space observer, equation (1) above must be integrated along the line of sight

$$I_{obs}^{sun} = \frac{1}{4} \int_{-\infty}^{\infty} \frac{3}{4} (1 + \cos^2\psi)\, \beta_o e^{-z} e^{-Ae^{-z}} e^{-t(z)} dx$$

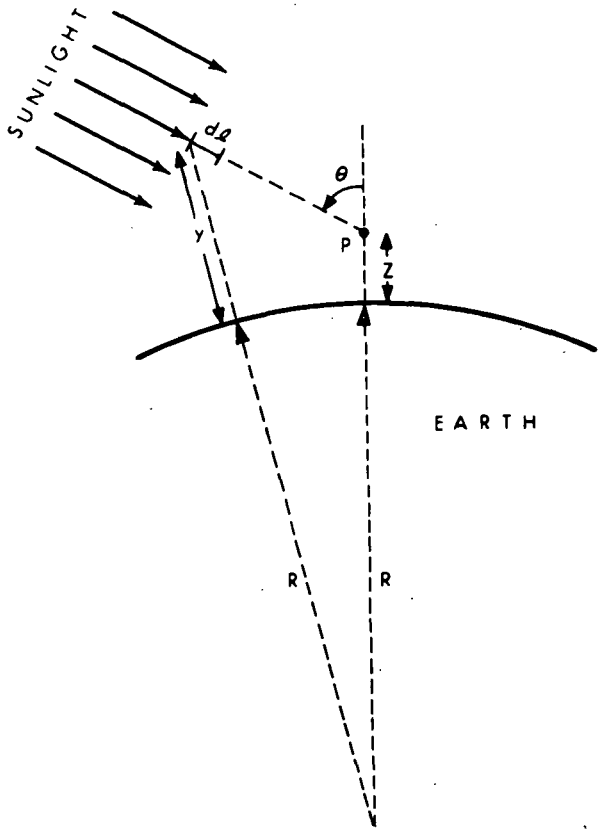

Diagram 1 Extinction of incident sunlight.

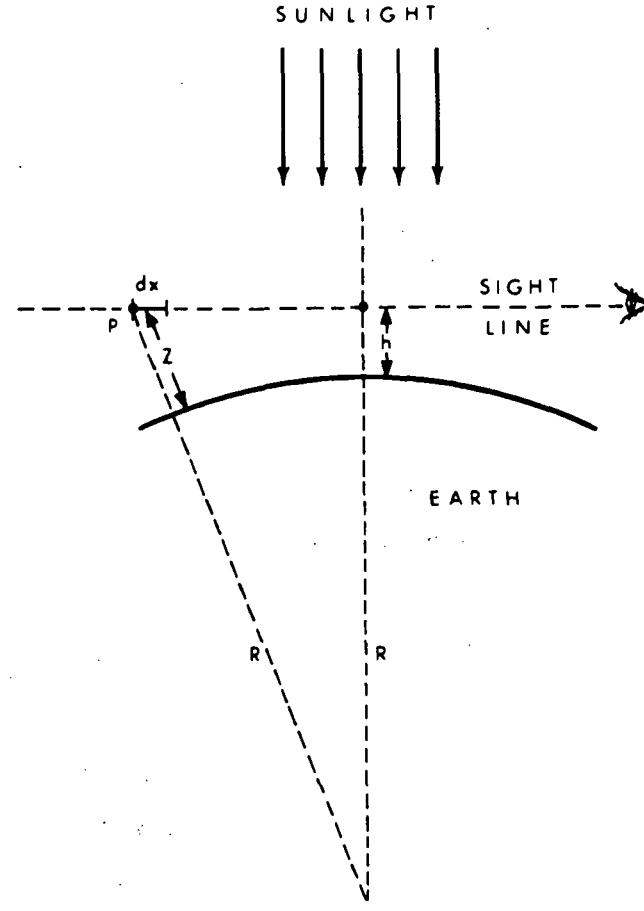

Diagram 2 Side view of diagram 2 showing extinction of scattered light seen by the outer space observer.

Figure 2

where the factor, $e^{-t(z)}$, is the attenuation of each light element from its scattering point to the observer along the sight line.. Appendix 2 of Reference (4) yields the optical thickness, t(z), between the origin and ± infinity,

$$t(z) = (1 \mp \text{erf}\sqrt{z-h}\,)\, Be^{-h}$$

where

$$B = \beta_o \sqrt{2\pi R}/2$$

Because x is a double-valued function of z, the integral must be summed in two parts, each taking a positive sign.

$$I = \frac{3}{16}\beta_o(1 + \cos^2\psi) \int_{-\infty}^{o} e^{-z-Ae^{-z}} e^{-(1+\text{erf}\sqrt{z-h}\,)Be^{-h}} dx$$

$$I_2 = \frac{3}{16}\beta_o(1 + \cos^2\psi) \int_{o}^{\infty} e^{-z-Ae^{-z}} e^{-(1-\text{erf}\sqrt{z-h}\,)Be^{-h}} dx$$

These can be converted to integrals over z by using, $x^2 \cong 2R(z-h)$, obtained from Fig. 2. Adding both integrals then yields

$$I_{obs}^{sun} = \frac{3}{8}\sqrt{\frac{R}{2}}\,\beta_o(1 + \cos^2\psi) \times \int_{h}^{\infty} \frac{e^{-(z+Ae^{-z} + Be^{-h})} \cosh(Be^{-h}\,\text{erf}\sqrt{z-h})\, dz}{\sqrt{z-h}} \qquad (2)$$

The above expression will later be combined with the scattered light which comes from the lower atmosphere.

2. Scattering of Light From the Lower Atmosphere

Light radiated upwards by the lower atmosphere is given by the tables of Reference 1 as a function of the zenith and azimuth angles of the radiation direction.

To calculate the amount scattered into the space observer's line of sight, each component of the tables must be separately calculated with its appropriate rayleigh factor. The total will be the sum of the separate contributions. In addition, the scattered light must be multiplied by a proper extinction coefficient and integrated along the line of sight. The result is

$$I_{obs}^{atm} = \frac{1}{4\pi} \int_{-\infty}^{\infty} \sum_{m=1}^{13} \sum_{n=1}^{16} \Omega_n \frac{3}{4}(1+\cos^2 \psi_m)\, I_{mn} \beta_o\, e^{-z} e^{-t}\, dx \qquad (3)$$

where the numbers 13 and 16 refer to the tabulated values of azimuth angle ϕ_m and zenith angle, θ_n, and I_{mn} are the tabulated intensity values.

The solid angle of each rectangular cone (which has intensity I_{mn}) is

$$\Omega_n = \Delta\phi \sin\theta \Delta\theta$$

$$\Omega_n = \frac{\pi}{6} (\sin\theta_n)(\theta_{n-1} - \theta_n)$$

The rayleigh scattering angle is given by

$$\cos \psi_m = \cos(\phi_m + \phi_o) \cos^2\theta_o$$

where ϕ_o is the azimuth of the space observer.

Examination of Equation (3) above shows that the summation factors are independent of z or x and may be brought outside the integral. The remainder inside may be directly integrated by the method of Appendix 3 of Reference 4. One obtains

$$I_{obs}^{atm} = \frac{3}{16\pi} \sum_{m} \sum_{n} \Omega_n (1 + \cos^2\psi_m) I_{mn}(1-e^{-2Be^{-h}}) \qquad (4)$$

where

$$B = \beta_o \sqrt{2\pi R}/2$$

For any given set of geophysical conditions Equation (3) reduces to

$$I_{obs}^{atm} = (\text{A constant}) \times (1 - e^{-2Be^{-h}})$$

This simple form is a consequence of the exponential density assumption for the upper atmosphere and the assumption of equal illumination for each point in the layer.

The net light received by the outer-space observer is the sum of Equations (2) and (4).

$$I_{obs} = I_{obs}^{sun} + I_{obs}^{atm} \qquad (5)$$

Equation (5) was evaluated using the Minneapolis-Honeywell 1800 computer and the resulting profiles are shown in Figs. 3 through 12.

ACCURACY OF RESULTS

Errors are divided into three categories:

1) Computational errors. These are the result of approximations made to simplify computation.

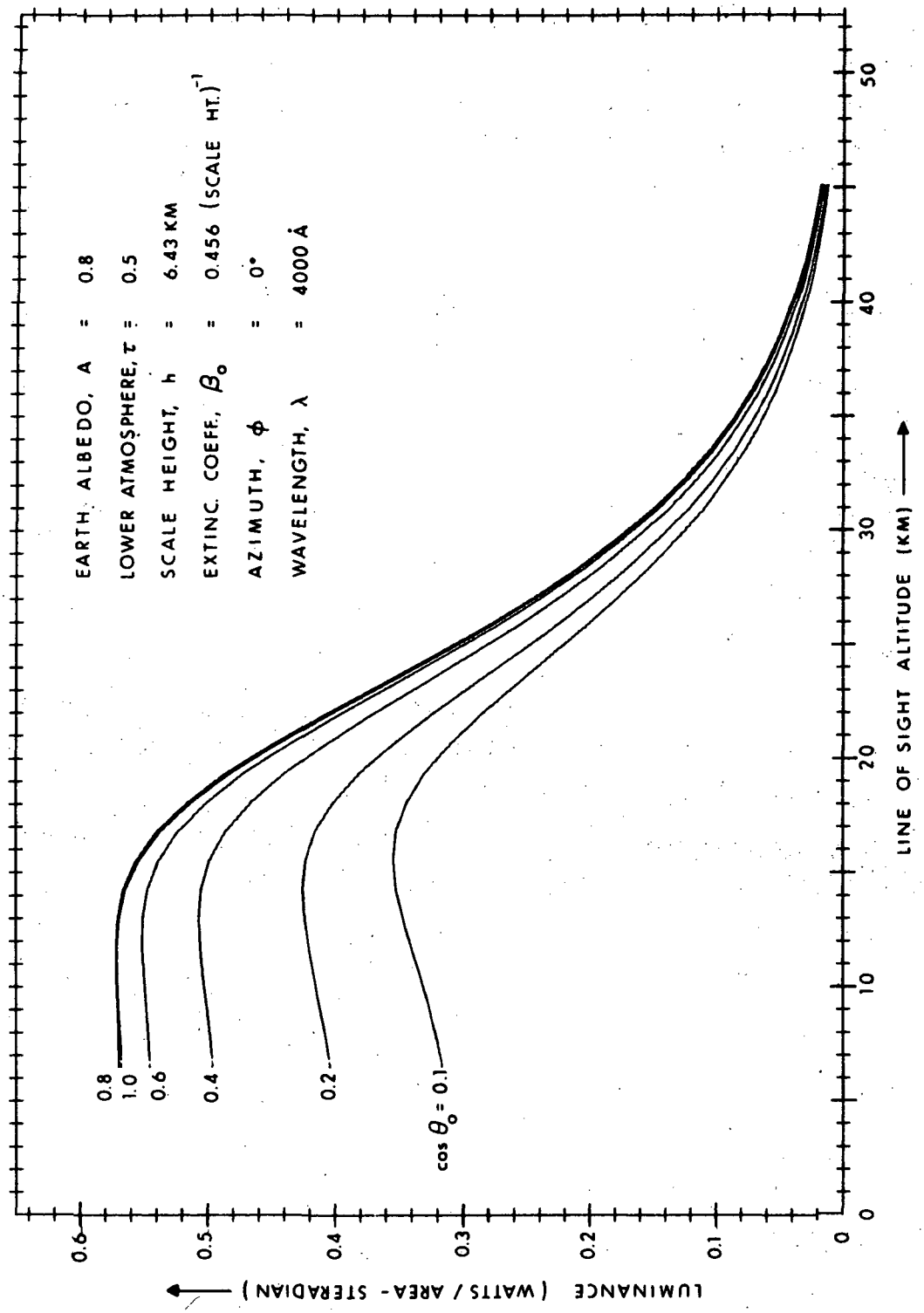

Fig. 3 Horizon profile showing effect of varying sun zenith angle and with albedo typical of total cloud cover.

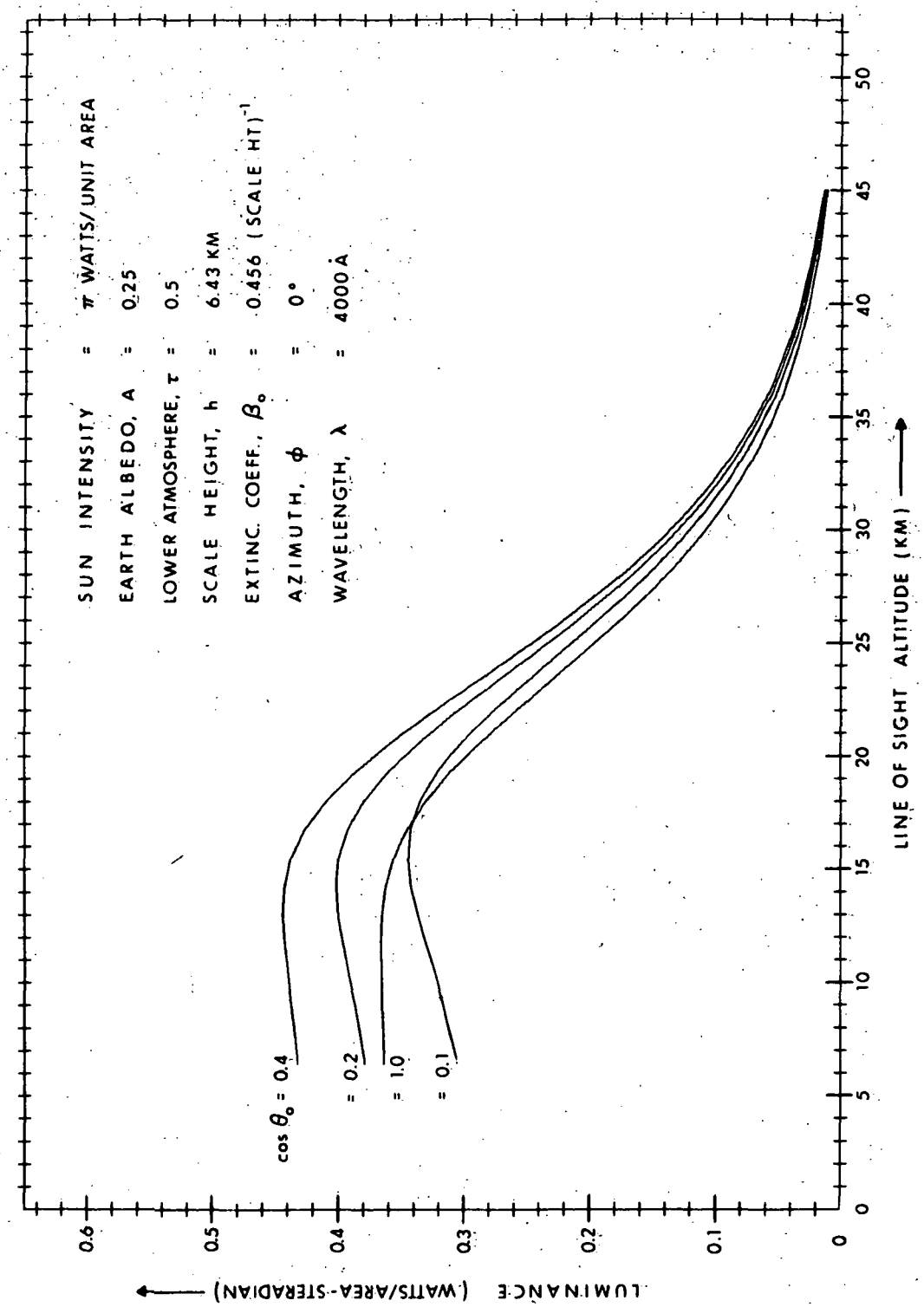

Fig. 4 Horizon profile showing effect of varying sun zenith angle and with albedo typical of light colored earth.

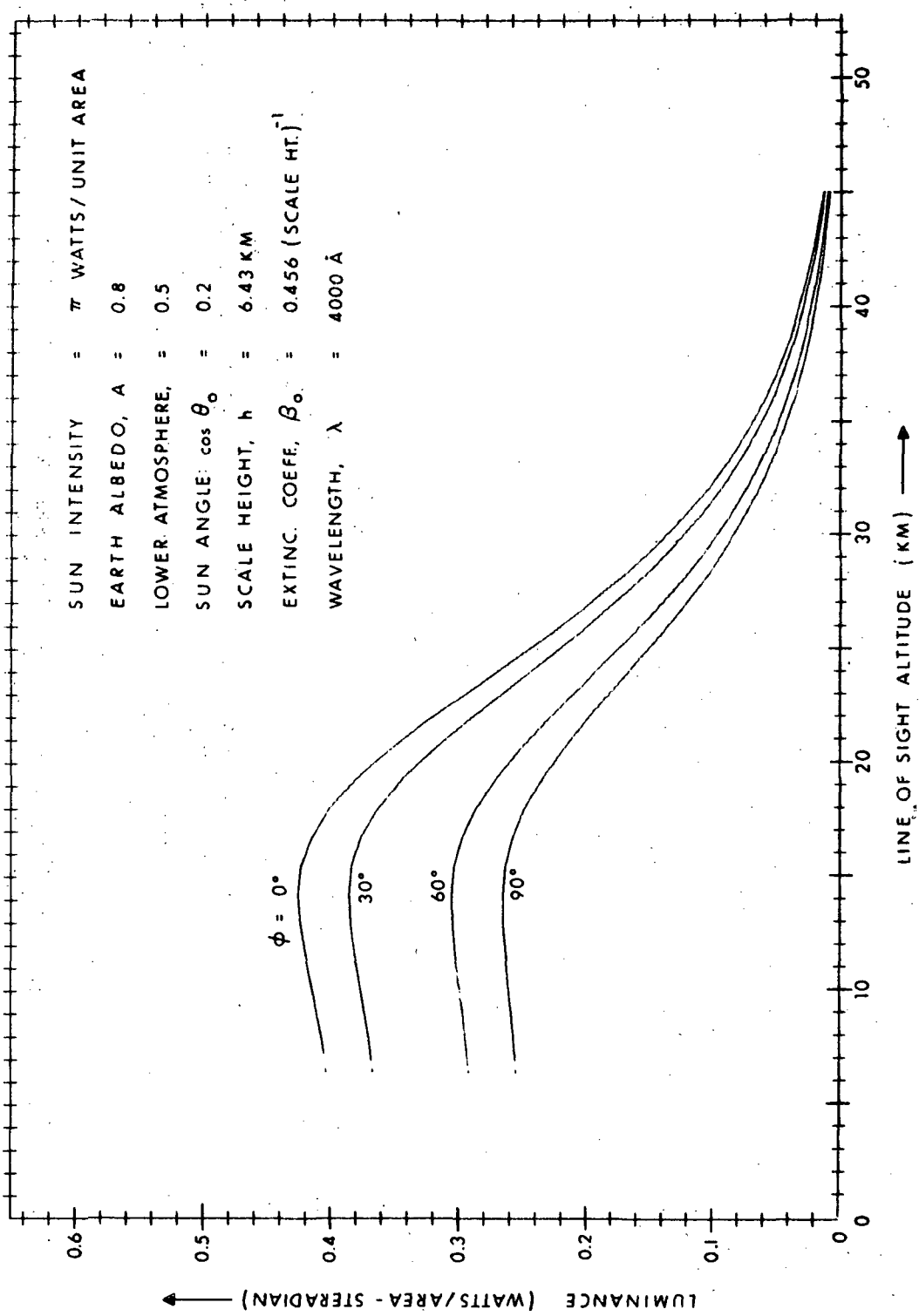

Fig. 5 Horizon profile showing dependence of observer's azimuth angle with respect to the sun's position.

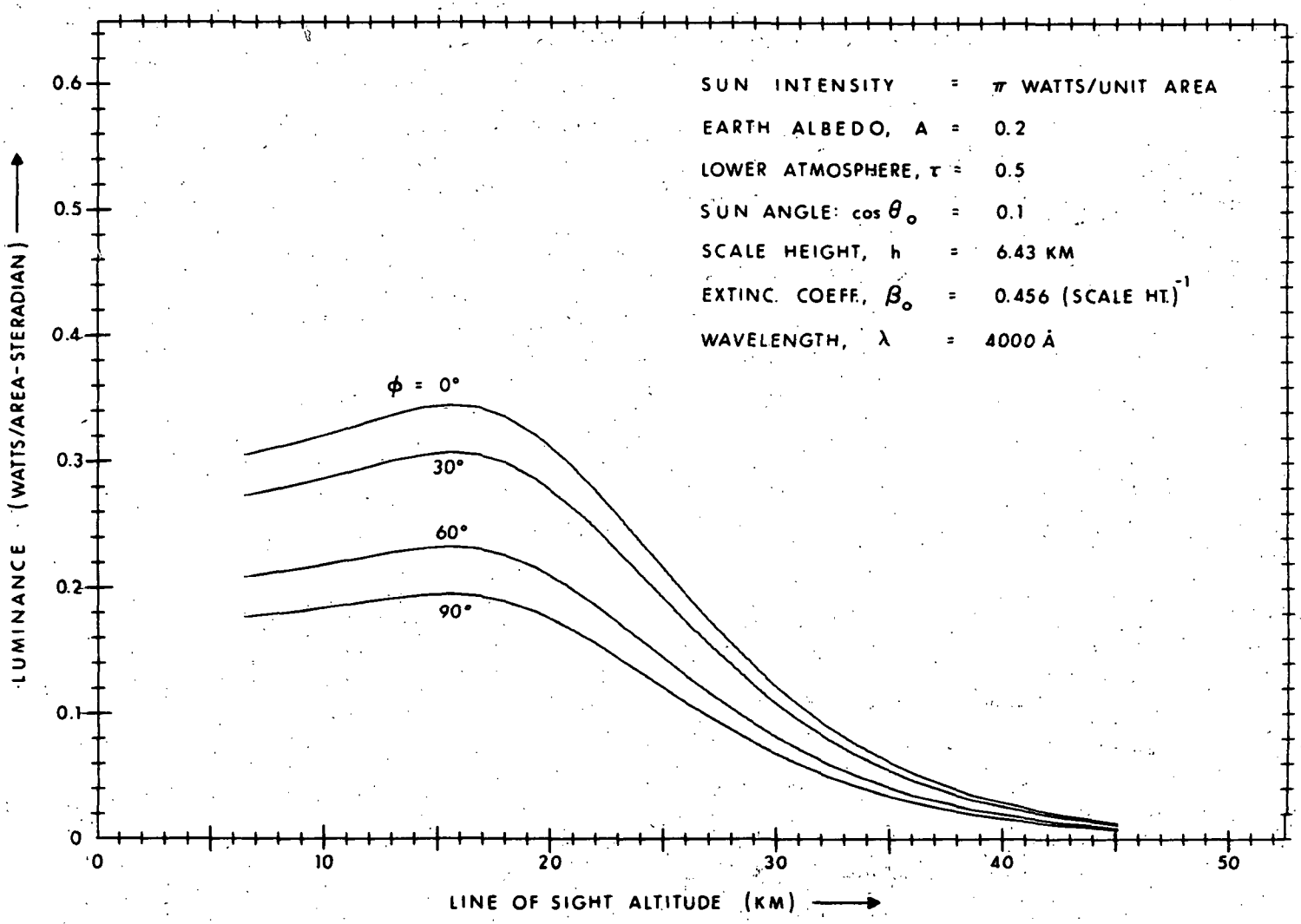

Fig. 6 Horizon profile showing dependence on the observer's azimuth with respect to the sun's position.

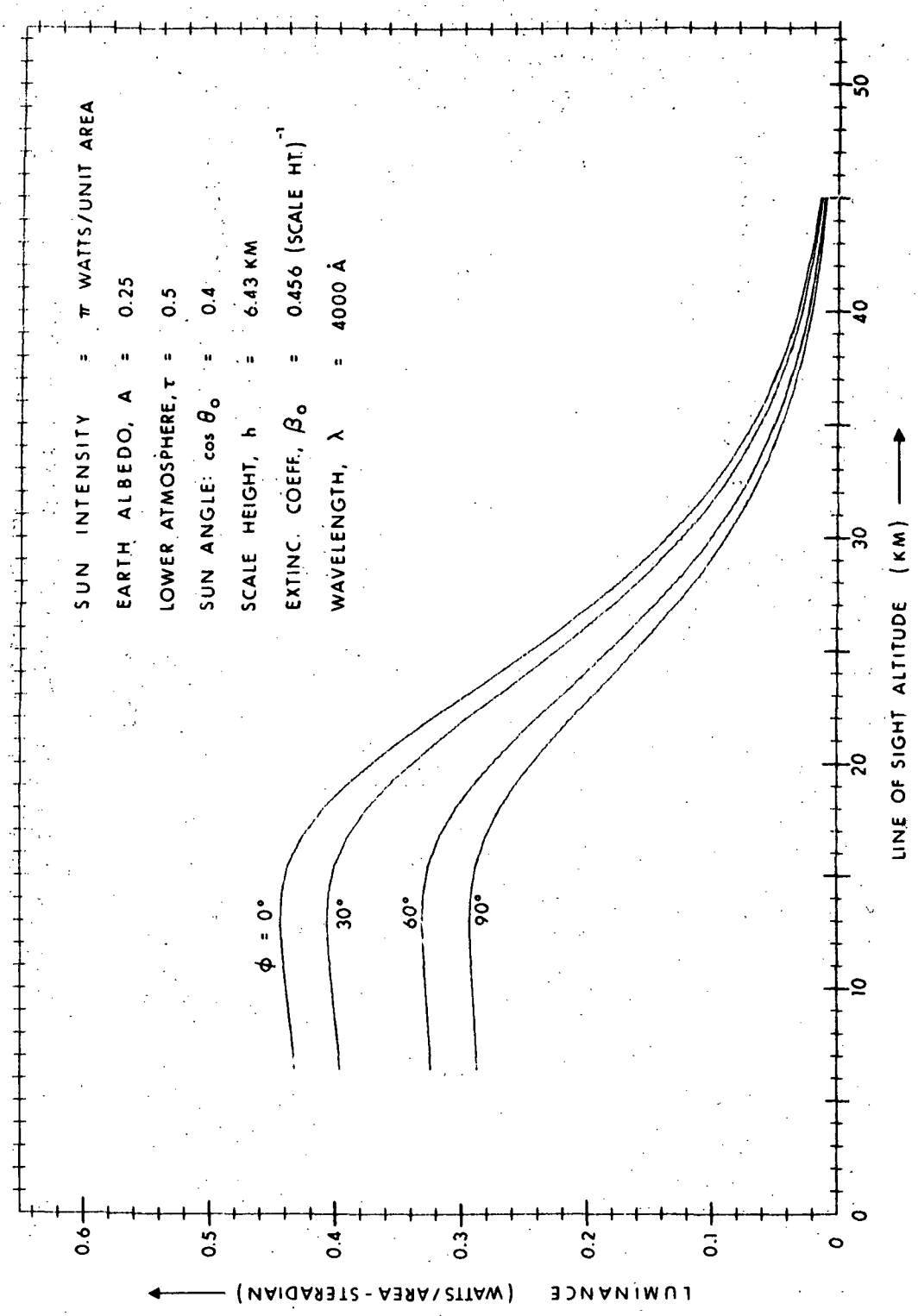

Fig. 7 Horizon profile showing dependence on observer's azimuth with respect to the sun's position.

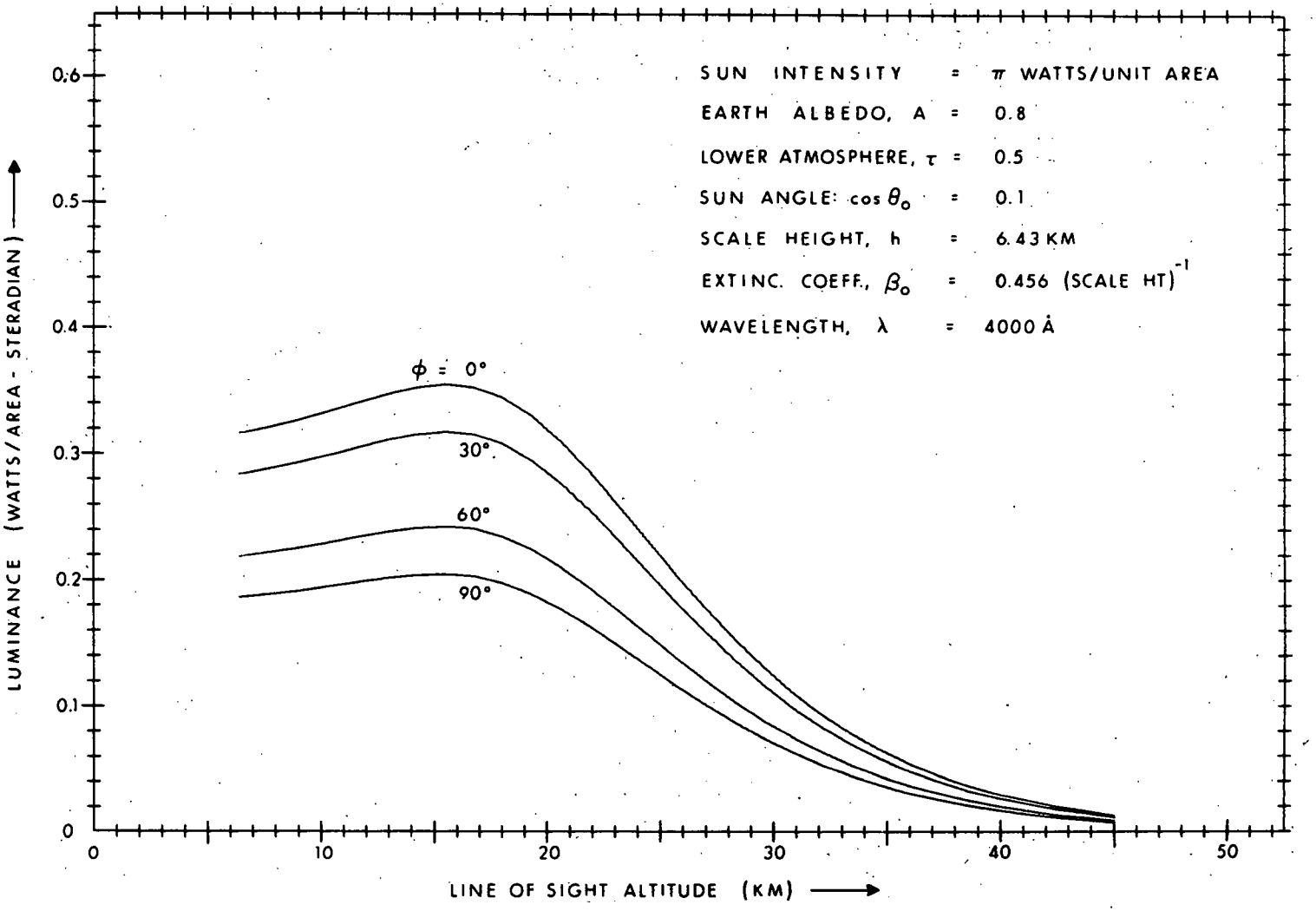

Fig. 8 Horizon profile showing dependence on the observer's azimuth with respect to the sun's position.

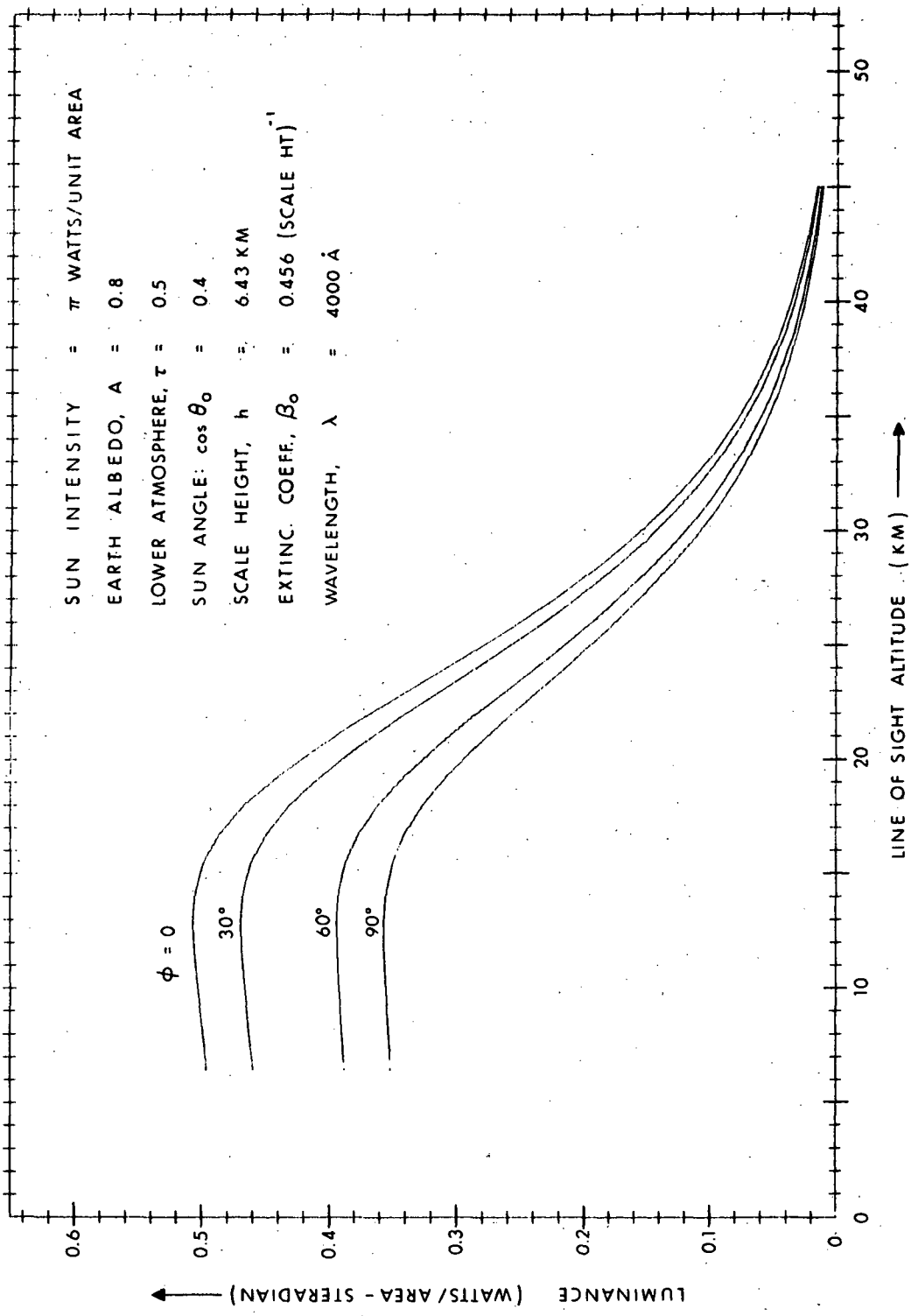

Fig. 9 Horizon profile showing dependence of observer's azimuth angle with respect to the sun's position.

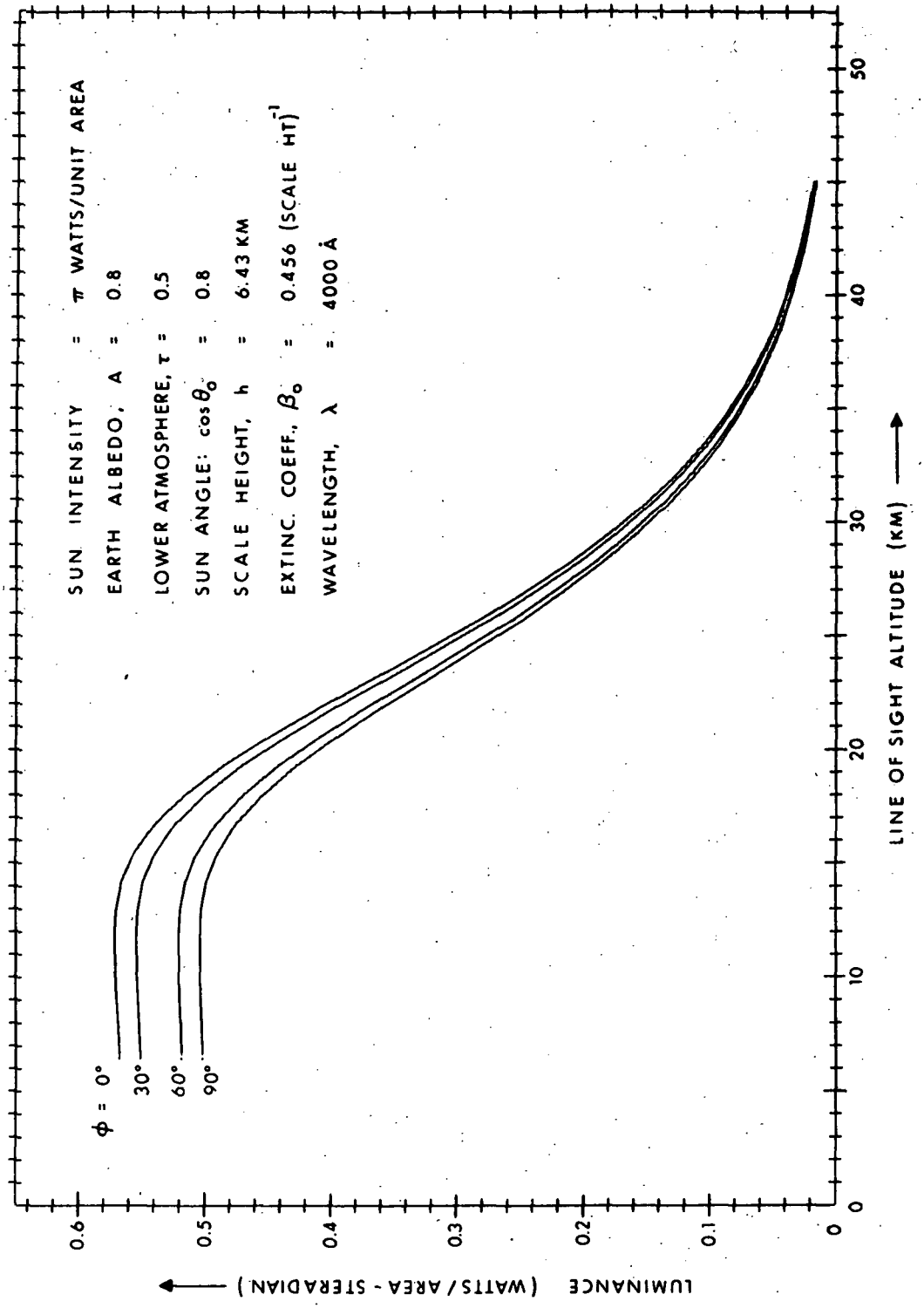

Fig. 10 Horizon profile showing dependence of observer's azimuth angle with respect to the sun's position.

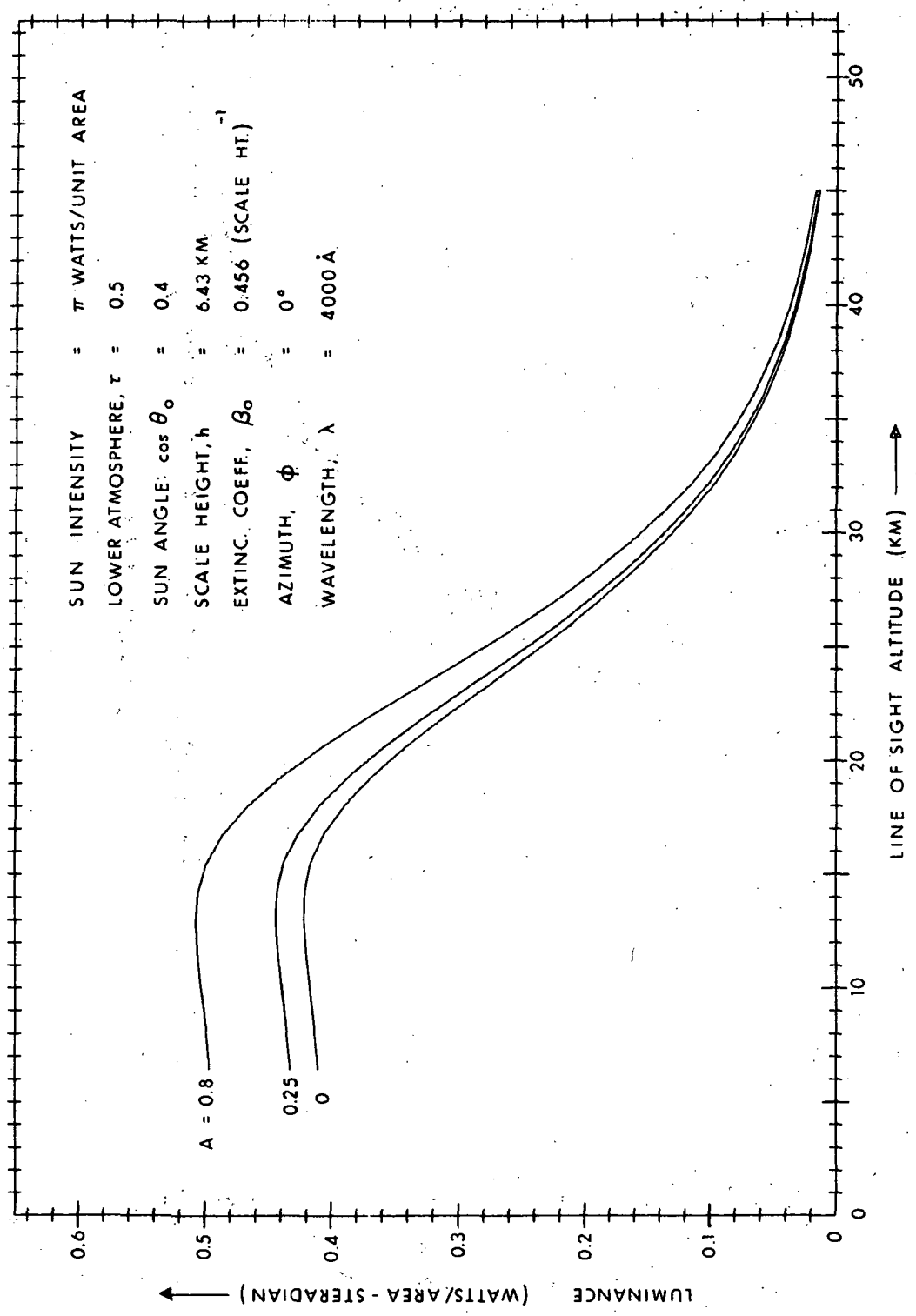

Fig. 11 Horizon angle showing dependence of ground albedo.

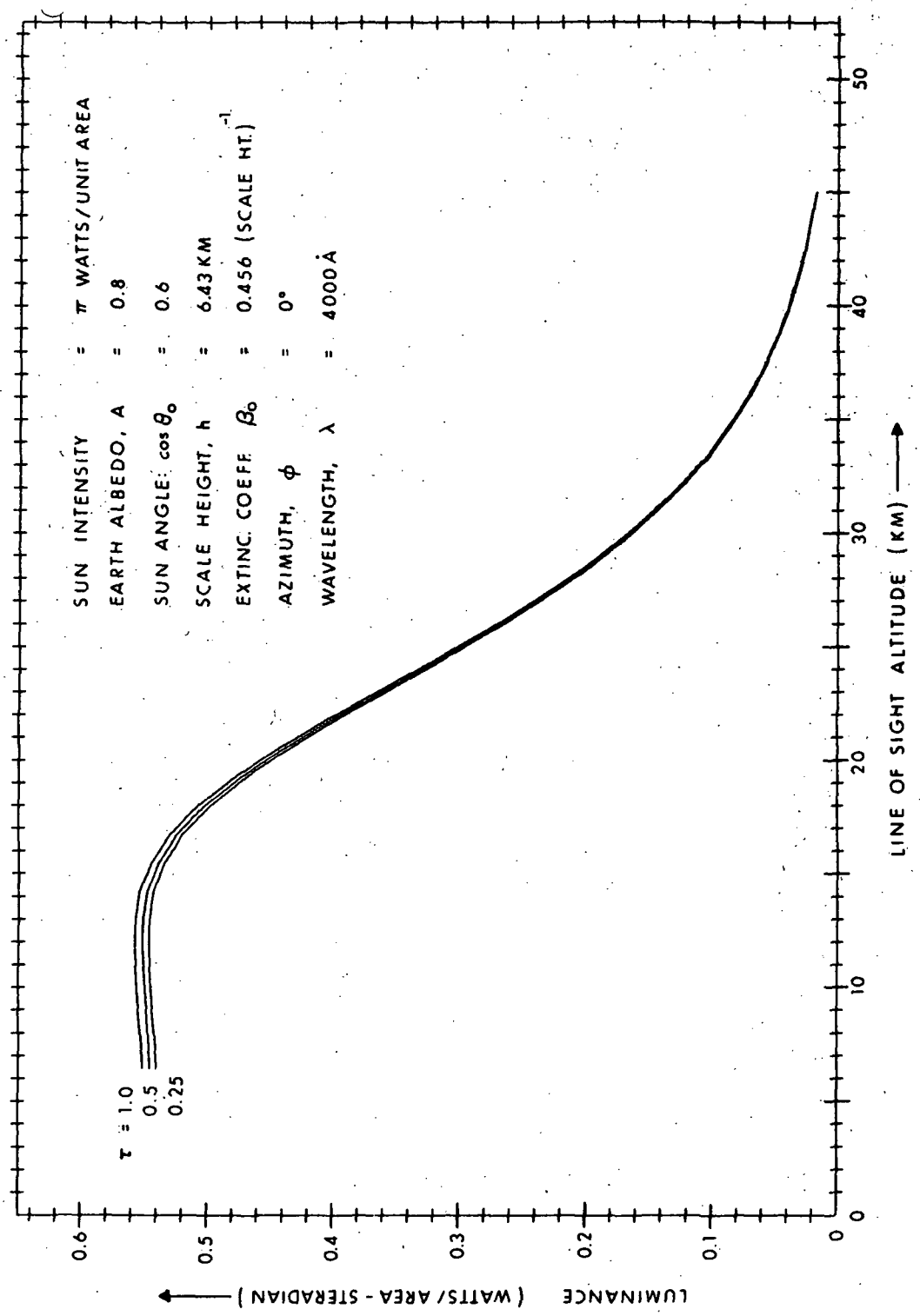

Fig. 12 Horizon profile showing effect of varying thickness of lower slab in the calculations.

2) Experimental errors. These are due to lack of precise experimental knowledge of the optical properties of the atmosphere.

3) Variability of Nature. These are caused by random temperature fluctuations, variation of ground reflectivity, etc.

1) Computation Errors.

To give a semi-quantitative idea of the probable accuracy of the foregoing computation, the error associated with various assumptions will be approximated and plotted as a function of altitude. By "error" is meant the percent deviation of the calculated profile intensity from the "true" intensity.

1.1 Equal illumination assumption.

The assumption is made that all depths of the upper atmosphere layer are equally illuminated by radiation from the lower atmosphere. A measure of the error caused is the percent extinction of an upward ray passing through the layer. However, because of the conservation of energy associated with the scattering process, no first-order error can appear. Second-order errors will be alterations of angular distribution and lack of energy conservation; both of which are complicated. To simplify matters, no specification of form is made, just

$$\text{error (1)} = \Delta I/I = \left[1 - e^{-\tau(h)}\right]^2$$

1.2 Neglect of Multiple Scattering in Upper Layer.

Multiple scattered sun rays which have not been accounted for are those which went through two or more scattering events into the upward hemisphere (the lower hemisphere has been accounted for). The probability of 3 or more events is negligible. The probability of two events is the product of the two probabilities.

$$\text{error (2)} = (1-e^{-\tau(\theta_o, h)})(1-e^{-\hat{\tau}(\theta_o, h)})$$

Note the similarity of form to error (1).

The first factor is the probability of a photon being scattered in an upper layer. The second event is more complicated since it depends on the angle of departure after the first event. The effective optical thickness, $\hat{\tau}$, is taken as

$$\hat{\tau} = \frac{1}{2\pi} \frac{3}{4}(1 + \sin^2 \theta_o)\beta_o e^{-h} \int_o^{\text{arc cos } 2/\sqrt{2\pi R}} \frac{\sin \theta \, d\theta \, d\phi}{\cos \theta}$$

$$= 2.8 \, (1 + \sin^2 \theta_o) \, \beta_o \, e^{-h}$$

The rayleigh angle has been approximated as a constant, $\sin \theta_o$, since most of the scattering will take place in a horizontal plane. The integral has been taken over a little less than $\pi/2$ because the earth's curvature prevents any ray from traveling horizontal by this amount. Error (2), the error of local illumination in the atmosphere, is plotted in Fig. 13.

The error of the profile intensity is the local error integrated over the line of sight and normalized to unity,

$$\text{Profile Error} = \frac{\int_{-\infty}^{\infty} (\text{Local Error}) \, I(x)\beta(x) \, A(x) \, dx}{\int_{-\infty}^{\infty} I(x)\beta(x) \, \mathbf{A}(x) \, dx}$$

where $I(x)$, $\beta(x)$, and $A(x)$ are the Illumination, scattering coefficient, and attenuation along the line of sight. This was computed and plotted in Fig. 14. Note that the large local errors at low altitude do not appear in the profile error. This because the space observer is unable to "see" deep down into the horizon atmosphere.

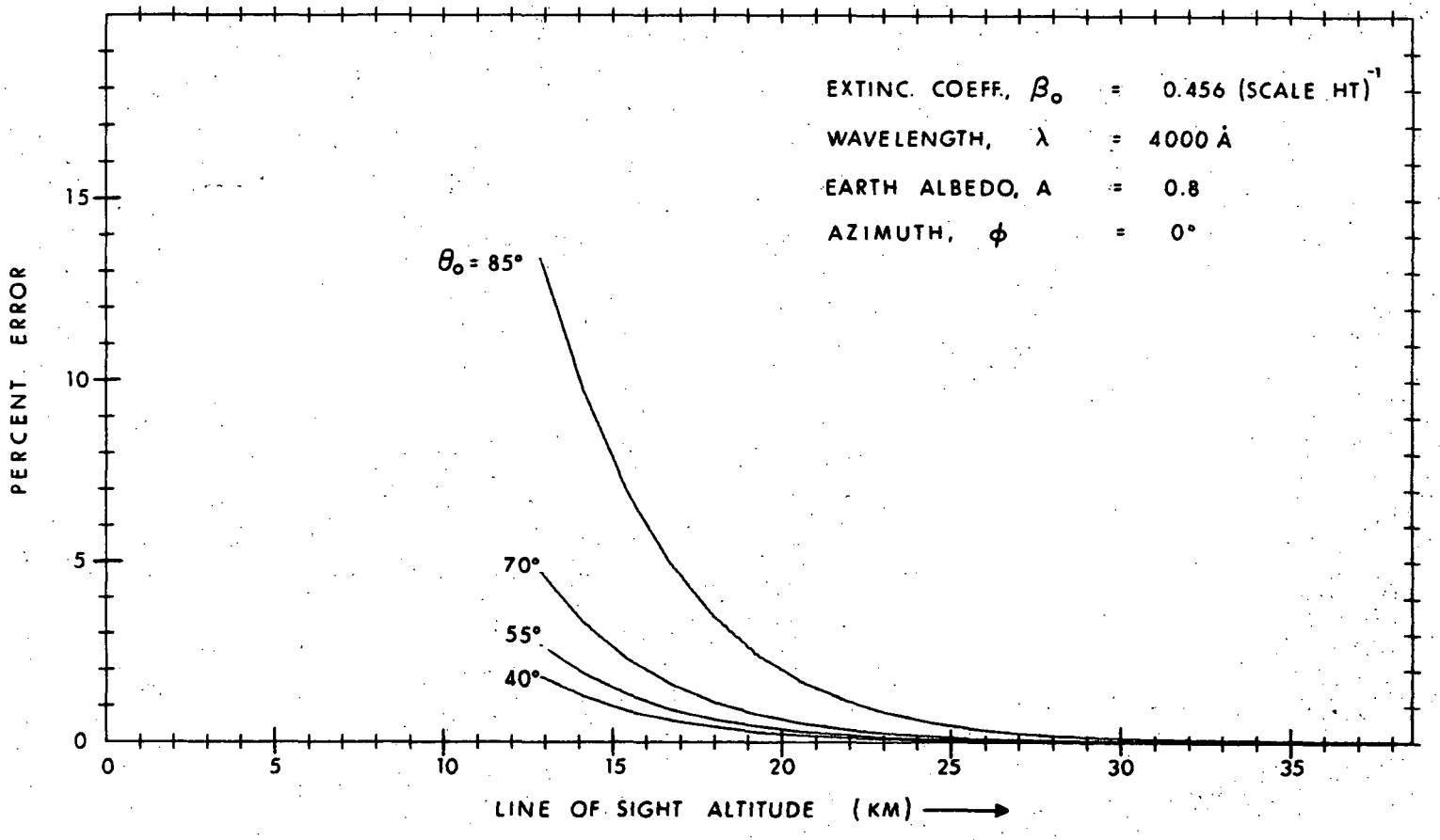

Fig. 13 Estimated error of the intensity of local luminance in the calculations as a function of altitude.

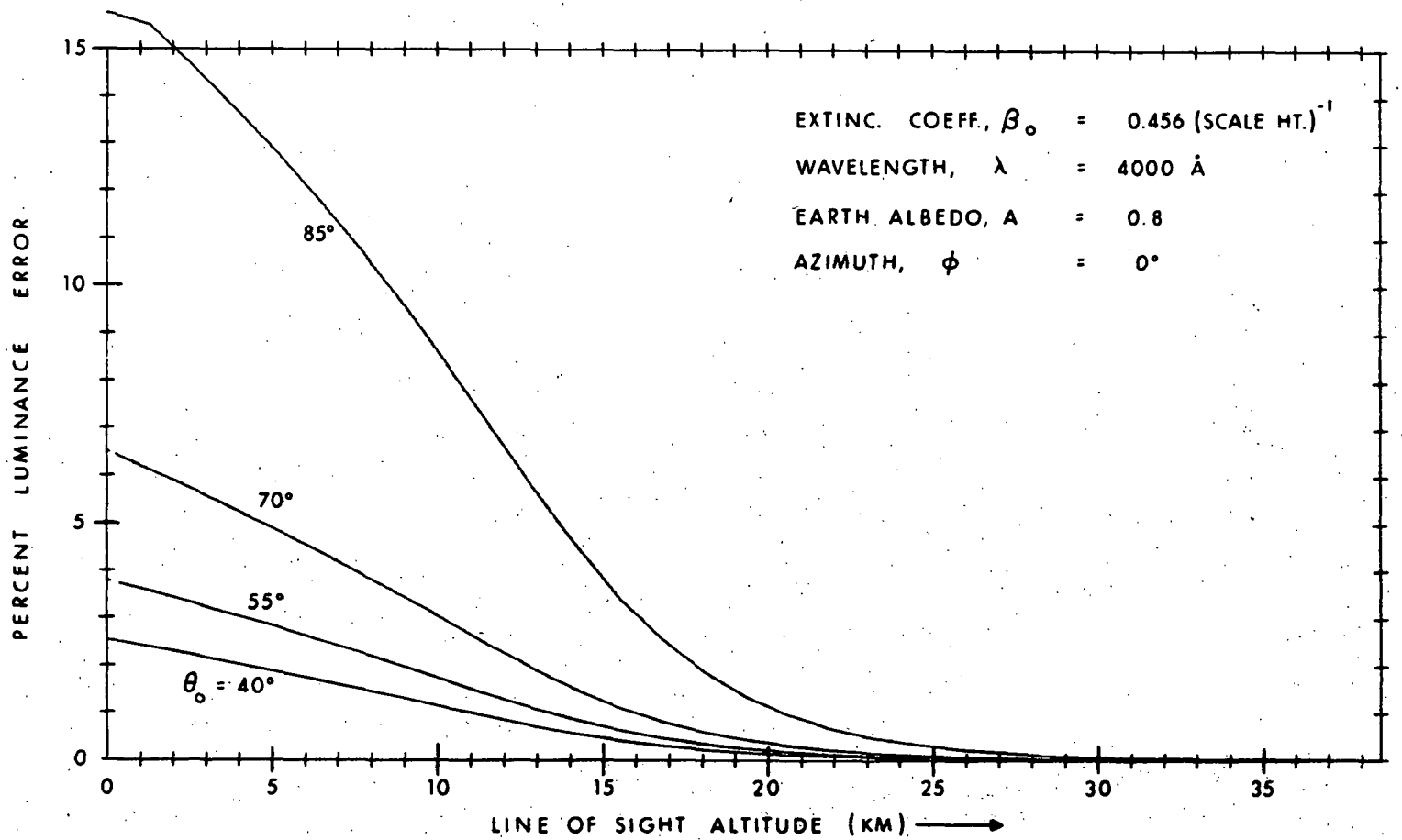

Fig. 14 Approximate percentage error of the profile luminance as a function of altitude.

2) Experimental Errors.

Essentially, this refers to the errors of Fig. 1 which represents the experimental data upon which any calculated profile must be based. The principal unknown in the upper layer is the aersol content which in Fig. 1 accounts for about 1% of the 0.4 micron optical thichness from 10 km upwards. If this were doubled, the shift of the half-maximum Luminance altitude would be about 0.2 km. However, not all investigators agree with Fig. 1. Fiocco[5] (1964) reports an aerosol layer at 20 km having an optical radar cross-section equal to twice the molecular cross-section. The layer has a half-thickness of 7 km. Newkirk and Eddie[6] (Jan. 1964) report extinction coefficients due to dust of value 10% of molecular at 12 km dropping to 3% at 20 km for wavelengths 0.44 micron. At present, it may be said that the unknown aerosols could effect the altitude of half-maximum luminance, by about a kilometer, at worst.

3) Variability of Nature.

The fluctuations of half-luminance altitude with temperature, pressure, and ground albedo were discussed in reference 4. Examination of Fig. 11 shows that the variability due to ground albedo must be revised downward, so that a summary appears,

VARIABILITY DUE TO:	LOCATION	
	EQUATORIAL	MID-LATITUDE
Temperature	± 0.2 km	± 0.8 km
Pressure	± 0.05 km	± 0.2 + 0.5 km
Albedo	< 0.1 km	< 0.1 km

The lower slab thickness is extremely dependent upon local weather and aerosols. Both are very difficult to anticipate in a real world. Nevertheless, if one assumes a 50% variability and then compares the curves of Fig. 12, which differ only in the choice of thickness, an intensity error of zero to 8% seems reasonable.

COMMENTS ON THE PROFILES

Figures 5 through 10 show the variation of profile according to the azimuth angle of the observer with respect to the sun. If the sun is in the zenith, the profile is the same all around the horizon. When the sun is low on the horizon, the profile is brightest when the sun is directly in front of or behind the observers, zero or 180°, respectively; and it is darkest when the obsever's azimuth is 90° or 270°. This effect is due to the rayleigh factor, $(1 + \cos^2 \psi)$, in the scattering process. Only one quadrant is shown, because profiles in opposite quadrants are almost identical.

Figures 15 and 16 show the relative amounts of horizon Luminance due to single scattering (the sun is the source), and multiple scattering (the lower atmosphere is the secondary source). Multiple scattering is dominant when the sun is in the zenith whereas single scattering dominates when the sun is low.

As the sun approaches the horizon, the maximum luminance increases due to an increasing rayleigh scattering function and also because less energy reaches the earth to be absorbed. But near the horizon these effects are overcome by the decreasing surface intensity of the sunlight. This is shown in Fig. 17 and also appears in Figs. 3 and 4.

NAVIGATIONAL CORRECTIONS.

If a navigational horizon is defined by a half-maximum luminance, additional accuracy can be obtained by a correction for the sun's zenith angle.

A more important, but not so obvious correction, involves determining the point of tangency of the line of sight on the ellipsoid of equi-gravitational potential. This is necessary because surfaces of equal atmospheric density are related to the ellipsoid rather than to a sphere. Neglect of this would lead to errors of the order of

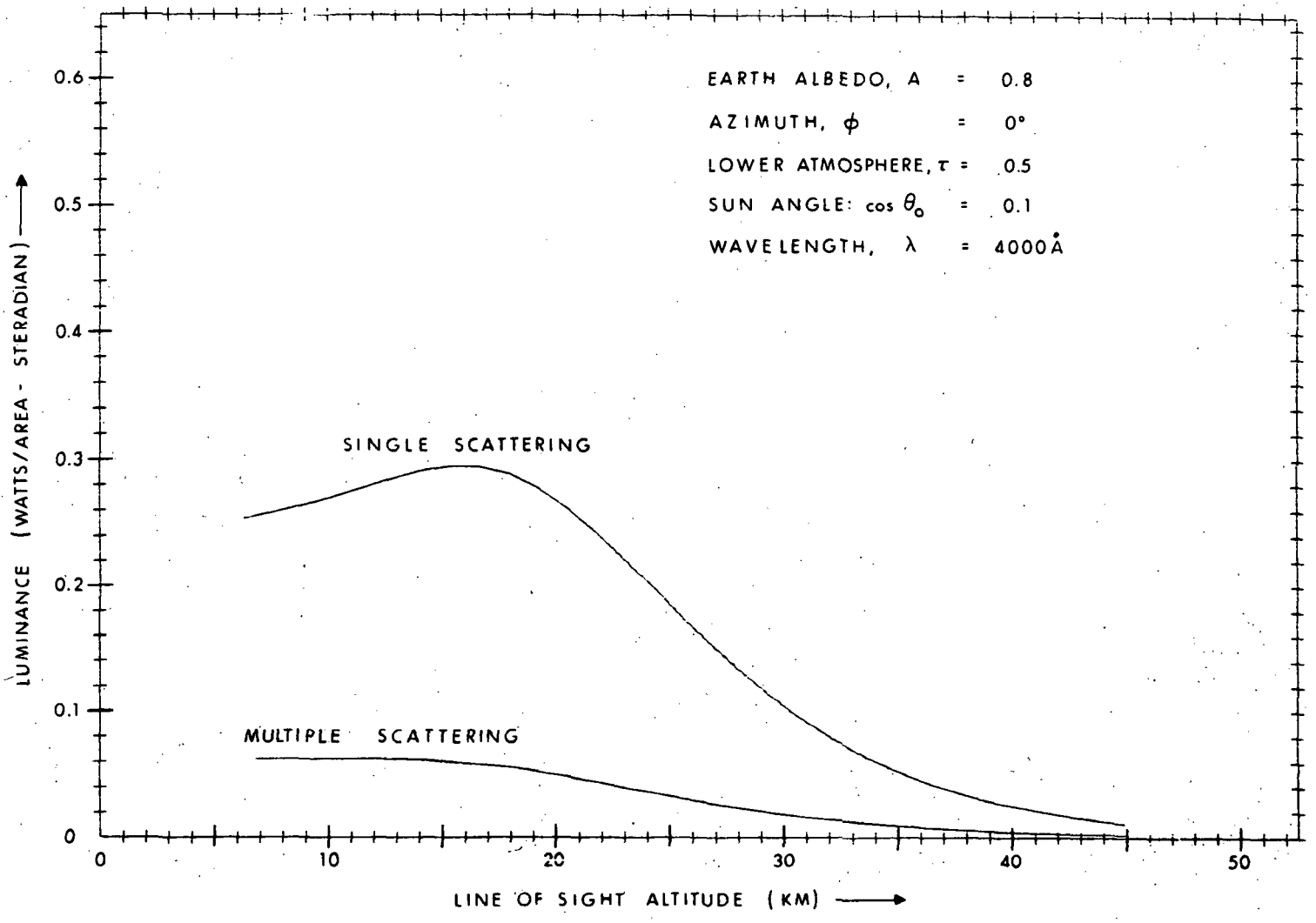

Fig. 15 Partial profiles showing the relative amounts of single scattering and multiple scattering that make up the total profile intensity.

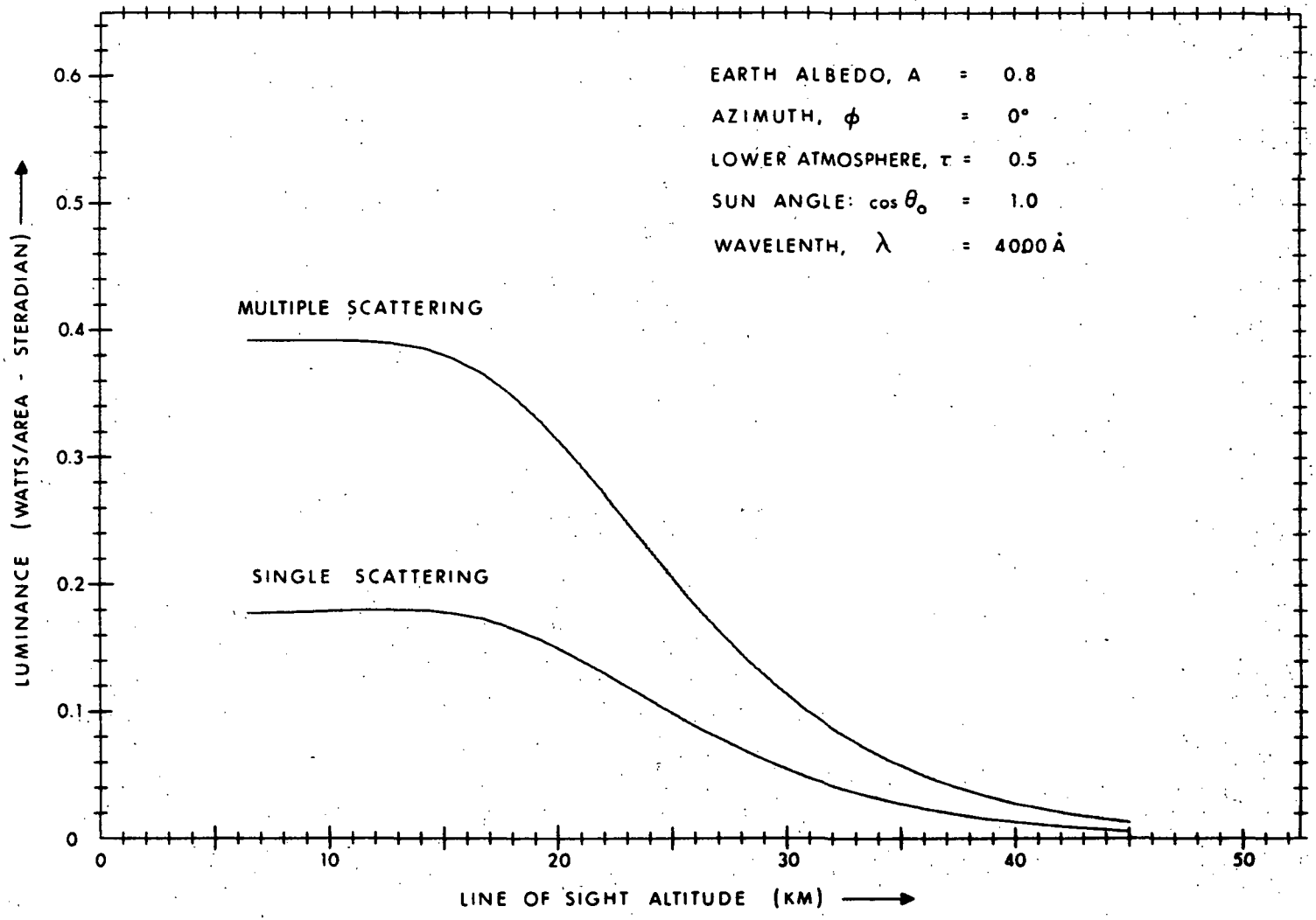

Fig. 16 Partial profiles showing the relative amounts of single scattering and multiple scattering that make up the total profile intensity.

the difference of the ellipsoid radii or about 12 kilometers. Thus a three-dimensional position calculation of an orbiting spacecraft using an earth horizon must include the approximate latitude and altitude of the observer. Corrections for sun zenith angle are shown in Fig. 18.

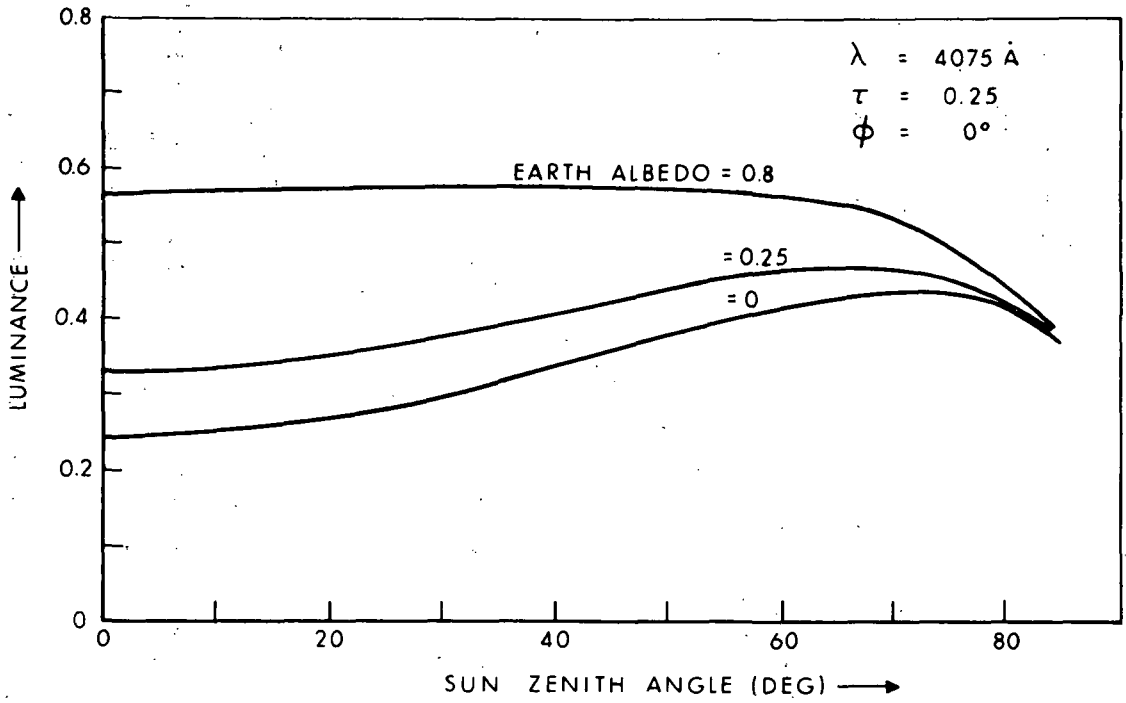

Fig. 17 Maximum intensity of horizon profile as a function of sun zenith angle.

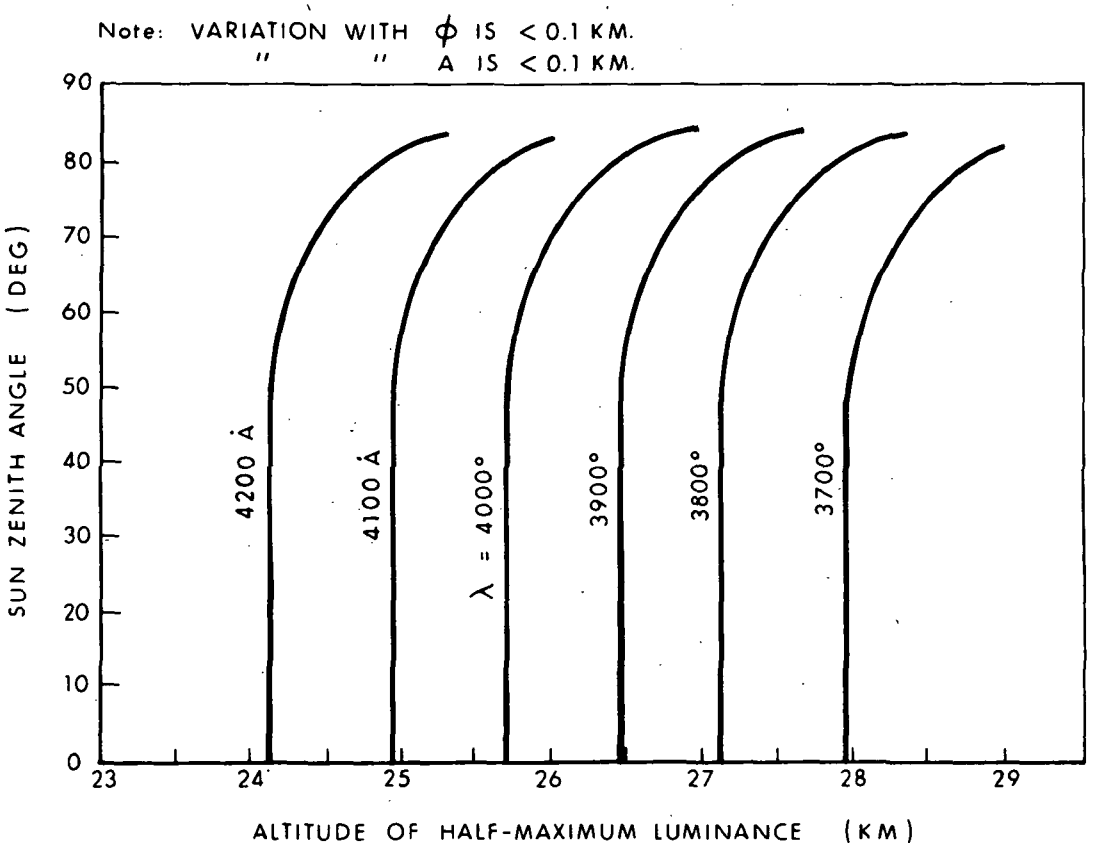

Fig. 18 Altitude of the half maximum luminance point taken from preceding figures and extrapolated for other wavelengths.

LIST OF SYMBOLS

μ	=	cosine of the sun's Zenith angle.
R	=	radius of the earth (in scale heights).
I_{obs}^{sun}	=	light scattered from the sun to the outer-space observer.
I_{obs}^{atm}	=	light scattered from the lower atmosphere to the outer-space observer.
x	=	length along the line of sight
z	=	altitude
ψ	=	rayleigh scattering angle, sun to observer.
ϕ_o	=	azimuth angle of observer with reference to the sun.
θ_o	=	zenith angle of sun.
h	=	altitude of sight line at closest point to earth.
ϕ_m, ϕ	=	azimuth angle of upward radiation from lower atmosphere.
θ_n, θ	=	zenith angle of upward radiation from lower atmosphere.

REFERENCES

1. Coulson, Dave, Sekera, "Tables Related to Radiation emerging from a planetary Atmosphere with Rayleigh Scattering", U. of Cal. 1960.

2. L. Elterman, "Altitude variation of Rayleigh, Aerosol, and Ozone Attenuating components in the Ultraviolet Region", AFCRL, 64-400, Hanscom Field, Mass. May 1964.

3. Court, Kantor, and Cole, "Supplemental Atmospheres", AFCRL, 62-899, Hanscom Field, Mass. September 1962.

4. Milo Wolff, "The Profile of an Exponential Atmosphere viewed from Outer Space and Some Consequences for Space Navigation," MIT/IL, Report E-1634.

Page intentionally left blank

Page intentionally left blank

E-1687

DISTRIBUTION LIST

Internal

M. Adams
R. Alonso
J. Arnow (Lincoln)
R. Battin
P. Bowditch
G. Cherry
E. Copps
R. Crisp
G. Cushman
J. Dahlen
E. Duggan
J. Dunbar
K. Dunipace (MIT/AMR)
J. B. Feldman
P. Felleman
S. Felix (MIT/S&ID)
J. Flanders
J. Fleming
F. Grant
Eldon Hall
D. Hanley
D. Hoag
A. Hopkins
F. Houston
L. B. Johnson
M. Johnston
B. Katz
A. Koso
M. Kramer
W. Kupfer
A. Laats
D. Ladd
J. Larsen
L. Larson
J. Lawrence (MIT/GAEC)
T. J. Lawton
T. M. Lawton (MIT/MSC)
D. Lickly
R. Magee
G. Mayo
J. McNeil
R. Mudgett
James Miller
John Miller
J. Nevins
J. Nugent
E. Olsson
C. Parker
W. Patterson
W. Schmidt
R. Scholten
E. Schwarm
J. Sciegienny
N. Sears
W. Shotwell (MIT/ACSP)
W. Stameris
J. Stone
J. Suomala
W. Tanner
R. Therrien
W. Toth
M. Trageser
R. Weatherbee
L. Wilk
M. Wolff (4)
R. Woodbury
W. Wrigley
Apollo Library (2)
MIT/IL Library (6)

External

(ref. PP1-64; April 8, 1964)

P. Ebersole (NASA/MSC) (2)

W. Rhine (NASA/RASPO) (1)

L. Holdridge (NAA S&ID/MIT) (1)

T. Heuermann (GAEC/MIT) (1)

AC Spark Plug (10)

Kollsman (10)

Raytheon (10)

Major W. Delaney (AFSC/MIT) (1)

NAA RASPO: (1)

National Aeronautics and Space Administration
Resident Apollo Spacecraft Program Office
North American Aviation, Inc.
Space and Information Systems Division
12214 Lakewood Boulevard
Downey, California

FO: (3)

National Aeronautics and Space Administration, MSC
Florida Operations, Box MS
Cocoa Beach, Florida 32931
Attn: HB 23/ Technical Document Control Office

HDQ: (6)

NASA Headquarters
600 Independence Ave., SW
Washington 25, D.C. 20546
Attn: MAP-2

AMES: (2)

National Aeronautics and Space Administration
Ames Research Center
Moffet Field, California
Attn: Library

LEWIS: (2)

National Aeronautics and Space Administration
Lewis Research Center
Cleveland, Ohio
Attn: Library

FRC: (1)

National Aeronautics and Space Administration
Flight Research Center
Edwards AFB, California
Attn: Research Library

LRC: (2)

National Aeronautics and Space Administration
Langley Research Center
Langley AFB, Virginia
Attn: Mr. A. T. Mattson

GSFC: (2)

National Aeronautics and Space Administration
Goddard Space Flight Center
Greenbelt, Maryland
Attn: Manned Flight Support Office Code 512

MSFC: (2)

National Aeronautics and Space Administration
George C. Marshall Space Flight Center
Huntsville, Alabama
Attn: R-SA

ERC: (1)

National Aeronautics and Space Administration
Electronics Research Center
575 Technology Square
Cambridge, Massachusetts
Attn: R. Hayes/A. Colella

GAEC: (1)

Grumman Aircraft Engineering Corporation
Bethpage, Long Island, New York
Attn: Mr. A. Whitaker

NAA: (15)

North American Aviation, Inc.
Space and Information Systems Division
12214 Lakewood Boulevard
Downey, California
Attn: Mr. R. Berry

GAEC RASPO: (1)

National Aeronautics and Space Administration
Resident Apollo Spacecraft Program Officer
Grumman Aircraft Engineering Corporation
Bethpage, Long Island, New York

ACSP RASPO: (1)

National Aeronautics and Space Administration
Resident Apollo Spacecraft Program Officer
Dept. 32-31
AC Spark Plug Division of General Motors
Milwaukee 1, Wisconsin
Attn: Mr. W. Swingle

WSMR: (2)

National Aeronautics and Space Administration
Post Office Drawer MM
Las Cruces, New Mexico
Attn: BW 44

MSC: (45)

National Aeronautics and Space Administration
Manned Spacecraft Center
Apollo Document Control Group
Houston 1, Texas 77058

Mr. H. Peterson (1)
Bureau of Naval Weapons
c/o Raytheon Company
Foundry Avenue
Waltham, Massachusetts

Queens Material Quality Section (1)
c/o Kollsman Instrument Corporation
Building A 80-08 45th Avenue
Elmhurst, New York 11373
Attn: Mr. S. Schwartz

Mr. H. Anschuetz (1)
USAF Contract Management District
AC Spark Plug Division of General Motors
Milwaukee 1, Wisconsin 53201